The heterogeneous electrical conductivity structure of the lower mantle

Pascal Tarits, Mioara Mandéa

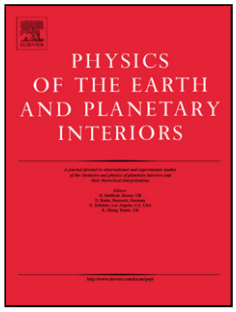

Title: The heterogeneous electrical conductivity structure of the lower mantle

Authors: Pascal Tarits, Mioara Mandéa

PII: S0031-9201(10)00156-1
DOI: doi:10.1016/j.pepi.2010.08.002
Reference: PEPI 5321

To appear in: *Physics of the Earth and Planetary Interiors*

Received date: 25-9-2009
Revised date: 2-7-2010
Accepted date: 13-8-2010

Please cite this article as: Tarits, P., Mandéa, M., The heterogeneous electrical conductivity structure of the lower mantle, *Physics of the Earth and Planetary Interiors* (2010), doi:10.1016/j.pepi.2010.08.002

The heterogeneous electrical conductivity structure of the lower mantle

Pascal Tarits*,[a], Mioara Mandéa[b]

[a] *UEB, IUEM, Place Nicolas Copernic, F-29280 Plouzané, France*
[b] *IPGP, Case 7011, 5 rue Thomas Mann F-75205 Paris Cedex 13, France*

Abstract

We developed a new three-dimensional electromagnetic time domain technique to invert 32 years of magnetic monthly mean values (1958-1990) from 120 geomagnetic observatories to image the mid-lower mantle. A preliminary global analysis of the data provided a source field model and an initial one-dimensional (1-D) conductivity profile for the inversion. The 1-D analysis showed that monthly mean magnetic data could resolve the lower mantle conductivity structure in the depth range $\sim 900 - 1400$ km. We run a series of synthetic data inversion to test the approach. The inversion of the true data with different initial conditions and different fractions of the data set was found fairly stable. Regions of low and high conductivity values were identified. The most resistive structures are beneath the Australian region, near Japan, North and Central America while highly conductive structures are identified beneath Eastern Africa and Eurasia. Some of these significant variations in the lower mantle conductivity are well correlated with structures in seismic tomography model. The uncorrelated features suggest

*Corresponding author
Email address: tarits@univ-brest.fr,mioara@gfz-potsdam.de (Mioara Mandéa)

that temperature and compositional effects known as predominant on both conductivity and velocity could be associated with other processes affecting mainly the conductivity, probably in relation with minor phases.

Key words: lower mantle conductivity, three-dimensional electromagnetic inversion, monthly mean geomagnetic data, lower mantle heterogeneities

1. Introduction

Estimates of the lateral variations of Earth's properties in the lower mantle come mainly from global seismic tomography. While great progress in lower mantle seismology models have been achieved recently (e.g., Romanowicz, 2003), interpretation of the seismic velocity anomalies in terms of thermodynamical and petrological parameters of the mantle is uncertain and needs additional information. The only other mean to directly probe the physical properties of the lower mantle is geomagnetic and geoelectric deep sounding to obtain the electrical conductivity. Conductivity is thermically active and sensitive to small amount of conducting material such as partial melting or water. Very recent progress in global and regional induction studies of the three-dimensional (3-D) earth provides new upper mantle conductivity models that may be quantitatively compared with other geophysical parameters (e.g., Kelbert et al., 2009; Utada et al., 2009). Most of known information on the lower mantle conductivity comes from one-dimensional (1-D) induction studies (Schultz and Larsen, 1990; Semenov and Jozwiak, 1999; Utada et al., 2003) and mineral physics (e.g., Shankland et al., 1993; Katsura et al. , 1998; Xu et al., 2000). From these studies a body of evidence has been assembled that suggests that the lower mantle is electrically heterogeneous.

A number of aspherical 3-D induction solutions have been developed in the last decade to address the issue of global heterogeneous mantle conductivity (see Kuvshinov, 2008, for a review) and a global inverse solution is recently proposed by Kelbert et al. (2008). Kelbert et al. (2009) are the first to propose a 3-D conductivity model of the uppermost lower mantle. The progress has been possible thanks to great improvement in computing systems and to increasingly larger data source, including satellite data. While the later are not yet included in 3-D inversion, the observatory data are being compiled for this purpose.

To infer conductivity distribution at lower mantle depth implies the use of very long reliable time series of geomagnetic and geoelectric data. Geomagnetic observatory data , geoelectric and geomagnetic time series or recent satellite magnetic data have been analyzed to obtain reliable geomagnetic data at the longest possible periods, typically a few months to 1 year (e.g., Egbert and Booker, 1982; Fujii and Schultz, 2002; Kuvshinov and Olsen, 2006). At these periods, the external time-varying magnetic field induces electric currents down to the mid lower mantle that in turn produce an internal magnetic field observable at the earth surface.

The time-varying geomagnetic field at these long periods is actually the superimposition of two types of sources, the internal secular variation of the main geomagnetic field by the earth's core dynamics and the interaction, external to the earth, between the sun and the main geomagnetic field. The external sources are organized at and within the boundary between the solar wind and the magnetic field (Courtillot and Le Mouel, 1988). When measured at the earth surface, the external magnetic field may be described with

simple geometry (Banks, 1969) namely an uniform continuously varying field which source is the ring current and two harmonic fields of period 6 months and 1 year. The field is also modulated by the 11 years period of solar activity. The external magnetic field induces electric currents in the conducting earth which in turn produces a magnetic field of internal origin. The later is a function of electrical conductivity to a maximum depth controlled by the skin effect. Electromagnetic (EM) induction analysis consists of the determination of the internal induced field and its interpretation in terms of conductivity structure.

We analyzed 32 years of monthly mean values of the geomagnetic field recorded at 120 geomagnetic observatories to obtain a new conductivity model of the mid-lower mantle. The strategy and methodology presented in this study were designed to analyze and model the observatory data to recover the lateral variation of lower mantle conductivity. The approach followed three steps. First, the data were globally analyzed to obtain a robust estimate of the external source field time series. Then, we carried out a 1-D inversion of the response function between the internal field and its dominant external dipole source. The 1-D conductivity profile was analyzed to infer the depth resolution of the data set and used as an initial model in the subsequent 3-D inversion. Finally, we ran a new 3D inversion scheme to derive the mantle electrical conductivity in the depth range acknowledged by the 1-D resolution analysis. The 3-D inversion was carried out in time and space domain. The rational to use a time and space domain approach compared to the usual spectral and spherical harmonic (SH) domain techniques was twofold. First, data are of various quality and duration. Several

observatories have been running for less than 32 years. Furthermore while an observatory is in operation, the control of the baseline to maintain continuity over time may have been uneven, creating spurious behavior in the data. Second, the geographical distribution of the observatories (Figure 1) limits considerably our ability to recover accurately the SH spectral coefficients related to mantle heterogeneity. The approach proposed here limits the spatial global analysis and attempts to match the actual time series at each observatory.

2. The source field and the 1-D earth

2.1. Data analysis

We assembled a new global data set of geomagnetic observatory monthly mean values (Table 1) from 1958-1990 (Figure 2). The data sources are the IAGA yearbooks and the national observatory archives. The data spatial distribution is given in Figure 1. The geomagnetic main field and secular variation model of Jackson et al. (2000) was removed from data. Spurious effects in the time seris are detected by time differencing the field (TDF). The TDF is also a high-pass filter that weights down long period residuals of the secular variation as well as the longest external source field such as the 11 years sun cycle. The TDF data file were edited. We inspected all the files to remove data with any spurious behavior. The editing was first carried out by hand with plot control. In general, we flagged any suspicious behavior in terms of continuity and lack of homogeneity in a given time series component compared to the other components and to observatories nearby (when existing). Whenever possible, we controlled the coherence between

a given component at an edited observatory with the same component at close observatories with no flagged values. At the end of the editing process, the final time series at some observatories were reduced and included gaps. Finally, three observatories (las, sba, crp, see Table 1) were removed from the database because of unclear and maybe spurious time changes in their time series.

In the period range of our time series, the external magnetic field may be described to a good approximation by a small number of SH coefficients (Banks, 1969). The continuum field and the 6 months harmonic field may be described by the first (degree $l = 1$) SH while the 12 months SH field is well described by the second spherical harmonic (degree $l = 2$). While higher odd spherical harmonic terms are also expected, the corresponding energy seems to decrease rapidly with the SH degree (Courtillot and Le Mouel, 1988). The skewness in the geographic distribution of the observatories is a major limiting factor in the derivation of the SH coefficients, particularly the internal field resulting from the mantle heterogeneities. Only the lowest order terms are in general accurately recovered because of the simple geometry of the source field. So we limited the SH analysis to degrees and orders up to 3.

Because the dominant dipole part of the geomagnetic field is tilted with respect to the geographic equator, it is best to analyse the data in the geomagnetic coordinate system. We used the 1960-1990 IGRF dipole to rotate the observatory locations and the horizontal magnetic components in this reference frame.

The global analysis approach takes stock of the simple geometry of the

source field to model the external field and the corresponding internal induced field. At and above the earth surface, the magnetic field is curl free and derive from a scalar potential $V = V_e + V_i$ (V_e external and V_i internal).

$$V(r,\theta,\varphi,t) = a\sum_{l,m}^{lmax_e}(r/a)^l V_{el}^m(t)Y_l^m + a\sum_{l,m}^{lmax_i}(a/r)^{l+1}V_{il}^m(t)Y_l^m \qquad (1)$$

where V_l^m are the SH coefficients of V. The function $Y_l^m(\theta,\varphi)$ is the spherical harmonic of degree l and order m at geomagnetic colatitude θ and longitude φ. The coefficient a is the earth radius and r the radius. The maximum degree of SH expansion $lmax_i$ is equal to $lmax_e$ for a spherically symmetric 1-D earth and larger for the 3-D case. The field $\vec{B}$ is obtained by taking the gradient of (1)

At each time step (one month) of the time series from 1958-1990, the potentials V_e and V_i were fitted to the observatory data in geomagnetic coordinates using Eq. 1. We tested various SH expansion models ($lmax = 1-3$ for the external field and $lmax = 1-7$ for the internal field). The system (1) for the magnetic field $\vec{B}$ was solved with a damped weighted robust least square method that minimizes:

$$M = \sum_{No} W_o\Sigma^{-2}|\vec{B_o} - \vec{B_c}|^2 + \lambda\sum_{l,m} l|V_{el}^m|^2 + (l+1)|V_{il}^m|^2 \qquad (2)$$

The subscripts o and c stand for observed and computed values. The first term in the right hand side of the equation is the misfit function. The weights Wo were obtained using the formalism proposed by Mochizuki et al. (1997) to make the observatory distribution uniform on average. The value Σ normalizes the field values to non-dimensional data and is taken arbitrarily equal

to 1 nT . The second term is the magnetic energy times λ, the damping parameter.

In spite of gaps in the time series either because the observatory was not running or because data were discarded, at any given time step there were data available from about simultaneous 60 observatories in the early years up to 115 in the latest years. We also tested the influence of the auroral observatories (geomagnetic latitudes larger than $\pm 65^o$ deg). We found that $lmax = 3$ provided a good fit on average to all observatories including the auroral's. In contrast, at periods shorter than 2 months Fujii and Schultz (2002) observe a strong auroral current effect down to rather low latitudes. We observe that this effect seems to vanish at our longer periods. The dominant zonal SH coefficients ($l = 1 - 3$) are shown in Figure 3. As expected, the ring current signal and the 6 months period field is dominant on P_1^0 while the 12 months period field is dominating the P_2^0 geometry. Note that these coefficients are for the TDF's so the 11 years sun cycle is only marginally visible.

2.2. The one-dimensional earth

In spherically symmetric approximation the ratio $Q = V_i/V_e$ in the frequency domain and at a given SH degree and order is the 1-D earth response function (e.g. Banks, 1969). The value Q as a function of frequency (or period) is used to obtain a 1-D conductivity profile of the earth. The dominant P_1^0 term is used because of its high signal over noise ratio. We obtained Q from the processing of the internal and external P_1^0 time series with a standard robust approach (Chave and Thompson, 1999). Prior to processing the periods 6 and 12 months were filtered out. The Q values were converted into

the classical induction length C (e.g. Olsen, 1999). The C values are listed in Table 2.

We used a non-linear inversion scheme (Hautot et al., 2000) adapted for a spherical symmetric solution to infer the a posteriori pdf on the conductivity model that best fit the data. The fit to the data is measured with a misfit function M of the form:

$$M = \sum_{Nf} \Sigma^{-2} |C_o - C_c|^2 + \lambda \sum_{i,j} [\log(\sigma_i/\sigma_j)]^2 \quad (3)$$

where the subscripts o and c stand for observed and computed. The first term in the right hand side of the equation is a χ^2 misfit. The value Σ is the standard deviation (Table 2). The regularisation (second term) damped by the parameter λ is based on the minimisation of the conductivity constrast between two different layers i and j.

The absolute minimum of χ^2 is $\chi^2 = 12.2$ for this set of data and was obtained for a Dirac distribution of conductances (Parker, 1980) (Figure 4). In our inversion, the earth was parametrized with a series of homogeneous shells to find the depth range resolved by the data. A datum (here Q or C) is representative of a certain depth approximatively given by the real part of C (Weidelt , 1972) We tested this estimation with models with different numbers of layers between 0-2400 km in depth. We observed that the data set were mostly sensitive to the conductivity in the depth range $\sim 1000 - 1400$ km. An example of an a posteriori pdf is presented in Figure 4a for a model with 5 layers. For this model the minimum misfit is 13.8. The conductivity is well resolved only between $\sim 1000 - 1400$ km with a value close to ~ 7 S/m. The data are weakly or not sensitive to the upper mantle conductivity.

Between $660 - 1000$ km, the conductivity may have any values less than $\sim 0.1 - 0.6$ S/m and below ~ 1400 km any value less than $\sim 3 - 10$ S/m. The deepest part of the mantle is conductive but its conductivity is not resolved either.

While the purpose of this analysis is mainly to prepare the subsequent 3-D inversion of the data, it is worth noting the large average conductivity value ($\sim 6 - 7$ S/m) in the depth range $\sim 900 - 1500$ km. This value is in general agreement with other global studies (see Kuvshinov and Olsen, 2006, and references herein) (Figure 4b). The conductivity value is also in agreement with the estimate of the mean mantle conductivity obtained by Mandea et al. (1999) deduced from the study of the diffusion through the mantle of the geomagnetic secular variation impulses. Depending on the thermodynamical conditions of the lower mantle (mineralogy, temperature, iron content, minor phase), mineral physics studies lead to large ranges of conductivity values (Verhoeven et al., 2008). Our estimates would suggest a hot mantle and/or large iron content.

3. Three-dimensional inversion

We have developed (Tarits et al., 1992) a forward 3-D spherical solver for induction to study the detectability of 3-D mantle conductivity (e.g., Tarits, 1994; Grammatika and Tarits, 2002). This solver was now implemented in an inversion algorithm adapted from the 3-D plane wave inverse solution of Hautot et al. (2000). The forward solver is in the frequency domain and calculates the electromagnetic (EM) field for an external (or internal) magnetic source input by its SH coefficients at a given frequency. The earth is parametrised

by a stack of shells which may be either homogeneous or laterally heterogeneous. The stack is limited downward by a homogeneous spherical core. In each heterogeneous shell, the electrical conductivity is given on a 2-D spherical grid. The conductivity is always in the space domain while the EM field is transformed forward and backward between space and SH domains in the numerical solution. The computed field is provided in the SH domain.

The inversion is based on the non-linear minimization of a misfit function M between the observed magnetic field and the computed magnetic field time series at each observatory plus a damping term to smooth the conductivity contrasts. The computed field is the response function of the conductivity model to the observed source field obtained before and used as forcing terms in the 3-D forward solver. The inversion technique minimizes M with a steepest descent approach adapted from the work of Beiner (1973). The gradients with respect to the parameters are not needed with this algorithm at a cost of a large number of calls to the forward solver. The number of calls is at least 10-20 times the number of parameters seeked in the inversion.

The misfit function M writes now:

$$M = \sum_{No} \sum_{t} W_o \Sigma^{-2} |\vec{B_o} - \vec{B_c}|^2 + \lambda \sum_{i,j} [log(\sigma_i/\sigma_j)]^2 \qquad (4)$$

The term $\vec{B}$ is the vector magnetic field (o for observation and c for calculated). The weight W_o are the same as in (2). The value Σ is the standard deviation taken here equal to $1nT$. The sum is over the number of observatory No and all time steps t. The regularisation term is the sum squared of all the log-conductivity contrasts in the model. The subscripts i and j designate the conductivity value in either cell or layer i or j. The damping

parameter is adjusted so that the damped reguralisation is smaller than the misfit. As a result, while the models obtained are not necessarily smooth, they do not exhibit spurious large conductivity contrasts.

One call to calculate the quantity M consists of the calculations of the induced field for all source field SH coefficients at all frequencies needed to restore the magnetic field time series at the earth surface. It is added to the external field and the total field is Fourier and Legendre transformed back into time and space domains at all observatory locations to calculate M. Note that all the calculations are carried out in the geomagnetic reference frame. The total number of data is:

$$NT = 3 \sum_{i}^{No} N_t(i) \tag{5}$$

where $N_t(i)$ is the number of data points in the time series at observatory i. The value of NT ranges from $48,000 - 110,000$ depending on the type of tests done on data inversion.

In order to obtain some benchmark for the approach proposed, we carried out a series of runs with synthetic data. The conductivity model considered was derived from the 1-D analysis presented before. A total of 4 layers over a homogeneous core were considered (Table 3). Only layer 3 is heterogeneous.

We designed a conductivity model with a checkerboard structure in layer 3 with the lowest conductivity values equal to the 1-D conductivity value (6.1 S/m) divided by $\sqrt{10}$ and the highest value equal to that 1-D conductivity times $\sqrt{10}$. The conductivity in layer 1,2 and 4 are those listed in Table 3. We simulated the magnetic field time series at all observatories and added 1 nT of noise. The source field is the one described in the previous section. The data

were synthetised on a grid much finer than the grid used for the inversion. We ran tests with different grids, different mesh sizes for the checkerboard and different inversion grids. Here we present a selection of results with the following characteristics. The data were synthesized on a 48x24 grid and the EM field computed with a maximum SH degree and order of 17. The checkerboard model has 16x8 meshes (Figure 5). The inversion grid is either the same size (Figure 5) or has 24x12 meshes (Figure 6). For the inversion the maximum SH degree and order was 9.

In the first example (Figure 5), the inversion grid is identical to the checkerboard model. The resulting inverse solution is very good despite the uneven distribution of data over the map. The polar regions however are not well recovered. During the inversion process (not shown here), the conductivity model was recovered progressively from the equatorial region to the polar regions in relation with the strength of the source field. In the second example presented in this study, the inverse grid was finer than the checkerboard model. As a result, the inverse grid did not coincide with the checkerboard's. The inverse solution in Figure 6 is therefore much more patchy than in the previous example. Again, the model recovery was driven by the equatorial-polar trend during the inversion. The final model in Figure 6 has not reproduced the polar regions at all. The areas with data are recovered with obviously some spreading of the conductivity values where the inverse grid meshes are over the boundary of two checkerboard meshes. In general, the conductivity contrast are well recovered when data are over such a boundary. The model has overshoot values in resistive regions.

The synthetic models were designed to test the ability of the time and

space domain algorithm to recover conductivity structures in the depth range 900-1400 km with synthesized observatory data. The tests run with various checkerboard sizes and inversion grid led to similar results. With coincidental grids, the model was always well recovered. The inversion with a grid that encompassed checkerboard mesh borders led to smeared structures which nevertheless agree reasonnably with the original conductivity distribution in areas with data. Finally we observed that the resistive regions were in general too resistive, an overshoot resulting from the sharp conductivity contrast between two checkerboard meshes.

4. Inversion of the observatory data

The inversion was initiated with a starting conductivity model identical to the initial model used in the study with synthetics. Again only layer 3 between 900 and 1400 km was heterogeneous. The analysis with the synthetic data suggested to use a 24x12 inversion grid and a maximum SH degree and order of 9. The parameters for the inversion are the conductivity in the 288 cells. Optionally, the conductivity in layer 1, 2 and 4 as well as their depth could be included in the inversion.

We carried out a series of inversion with different initial models and different sets of data. In all inversions, the regularisation term in (3) was set to about 1-10 % of the misfit term. In all trials, we observed that the auroral observatories could not be well fitted in spite of the presence of the 6 months and 1 year source terms. As a result, we removed 5 observatories with geomagnetic latitudes higher than $\pm 75^o$ deg (Table 1). Note that the data set is in the geomagnetic reference frame for the inversion.

All runs led to similar patterns in the conductivity structure. A typical run is presented in Figure 7. The 1-D initial model explained a large fraction of the time series, in particular the North component X which carries a dominant source field. The inversion was stopped when no significant changes were observed, roughly after ~ 5000 calls to the forward solver. The misfit decreases monotonically with regular jumps when a general new conductivity pattern is obtained. The occurrence of this pattern is visible in the regularisation parameter. This pattern is obtained after all directions for all parameters have been explored and the steepest slope found for the misfit function M. We found the Y component the most difficult to fit (Figure 8). In the equatorial region, the Y amplitude is quite large compared to the model response. There might be some source field residual. The X component is in principle not very discriminatory for the conductivity structure because the source field is dominant in this component. But it is in general very accurately measured and is therefore very useful. Both components Z and Y carry a large fraction of the induced signal and are therefore discriminatory although Z is in general more noisy than the horizontal components. These observations are summarized in Figure 9. The values presented in Figure 9 are the differences between the rms of the final solution and the rms of the starting 1-D solution for each observatory. The rms is defined by:

$$rms = \sqrt{\frac{3}{NT} \sum_{No} \sum_{t} \Sigma^{-2} |\vec{B_o} - \vec{B_c}|^2} \tag{6}$$

for each component X, Y, Z. Most of the rms decrease is observed in Z while in several stations X may increase, probably in relation with uncertainties in the source field. It is difficult to estimate the impact of the source field

errors in the results. One possibility is to use different parts of the data time series because the source field is calculated independently at each time step. The results discussed below suggested that this impact might be small.

We present two cases with different runs. The first case (Figure 10) results in models with two different initial 1-D conductivity values in layer 3 (6.1 S/m and 1.8 S/m). In the second case (Figure 11) we split the data in two. One set was from 1958-1974 and the second set was from 1975 to 1990. Both inversion started with a value of 1.8 S/m in layer 3. The models in Figures 10-11 are presented without any interpolation. We also tested (not shown here) the influence of the conductivity values in layer 1, 2 and 4 as well as the thickness of layer 3 with a run in which these parameters were included in the inversion. The conductivity values in those layers were unstable and varied according to the pattern in Figure 4. The thickness changed by about 50-100 km without change in the layer 3 conductivity structure.

In case 1 (Figure 10), we observed that the largest scale structures were always reproduced with slightly different conductivity values. The conductivities were somehow dependent on the choice of the initial values. The final model with an initial conductivity value of 1.8 S/m in layer 3 is overall more resistive than the final model with an initial value of 6.1 S/m. We have averaged the two models (Figure 10). In a given mesh, the conductivity value $\overline{\sigma}$ is the arithmetic mean of the conductivity from both models. We calculated the relative difference Δ in each mesh of the grid between both models as follow:

$$\Delta = |\sigma_1 - \sigma_2|/\overline{\sigma} \tag{7}$$

where σ_1 and σ_2 are the conductivity value in one mesh for each model.

These relative differences (Figure 10) are the largest in the polar region and in areas with no data. The pattern in the relative difference map is however complicated. Some regions with no data inside but with data on the border have weak differences while regions with some data inside have significant values. These differences are probably caused by several factors, the maximum SH degree cut off, the distribution of observatories as well as a moderate level of regularisation in the misfit function M in equation (3).

In case 2 (Figure 11), the final model with the 1958-1974 data set is the result of a smaller number of observatories (60-90) and shorter time series than for the 1974-1990 data set (80-110 observatories). The model is also smoother than the model obtained with the 1974-1990 data set although all the main features are observed in both models. One likely contribution to the differences between the 1958-1974 and 1975-1990 models comes from the uncertainty in the source field model used. The comparison between these models and the full data set (1958-1990) model in Figure 11 showed that both 1958-1974 and 1975-1990 data contributed.

5. Discussion

On the basis of the analysis carried out with synthetic data, we attempted to draw some conclusions about the resolution and uncertainty in the lower mantle (LM) conductivity model we obtained. Despite the uneven distribution of observatories, the synthetic tests showed that LM conductivity contrasts were correctly recovered. The conductivity structures were grid dependent and smeared over the actual LM bodies. Furthermore, the resistive regions tended to be undershoot. On the bright side, the stability observed

in the various inversions of the real data carried out with different settings suggested that at least the large scale structures might be robust features of the model. The models in Figure 12 are a smooth version of the model in Figure 10. We expanded the conductivity values in SH and we recalculated the conductivity distribution for different ranges of SH degrees and orders to outline the structures that dominated at long wavelength. There are several salient features in this model. We observe areas of low conductivity beneath the Australian region, Western Africa, near Japan, North and Central America. High conductivity is observed in Eastern Africa, South-East Asia and Eurasia. The low conductivity values observed in the Pacific ocean seems resolved while the N-S extension of the Western Africa low conductivity region is probably an artefact caused by the very small number of observatories along the African coast.

The conductivity value obtained from the inversion of induction data is in principle absolute although not necessarily well resolved. The value is representative of the conduction mechanism in the lower mantle. There is some sense to discuss the conductivity distribution in terms of high and low values compared to a mean 1 S/m (Figure 12). A number of 1-D global studies (Kuvshinov and Olsen, 2006) shows a value of 1-2 S/m for the mean conductivity in the 1000-1500 km range. Mineral physics studies, using average mantle temperature and composition conditions, show similar values (e.g., Xu et al., 2000).

The resistive regions in the model are likely to show values too low if we referred to the synthetic analysis. We do not really know by how much the value is too low. It could be a factor of 2 or 3 according to the results

presented in Figure 6. In contrast, the synthetic analysis showed that the conductivity in high conductivity regions (Figure 6) should be of the right value. Some of the conductivity values are large (more than 10 S/m) which agreed with the 1-D conductivity profile obtained with the global earth response of Table 2. Eventually, what might probably be the most robust parts of the models in Figure 12 are the high and low conductivity regions but their exact size, shape and conductivity could not be very well defined. The worldwide variability of our conductivity values are in agreement with the few deep 1-D conductivity profiles obtained with different type of EM data (Egbert and Booker, 1982; Schultz et al., 1993; Semenov and Jozwiak, 1999; Utada et al., 2003). We observed significant discrepancies between our model and the conductivity distribution proposed by Kelbert et al. (2009) in the same depth range. Their model shows a weaker conductivity contrast (1 log unit or less) than our model. This result is not surprising given the widely different approach used, in particular for the smoothing parameterization and the fact that our technique may produce conductivity too low in resistive areas. More problematic is the absence of some of our prominent features in Kelbert et al.'s model. For instance, the Australian low does not exist neither does the Japan low. In contrast, our models are in good agreement from Southern Europe to Middle East as well as Eurasia. One possible explanation lays in the short period data set (maximum period 100 days) used by Kelbert et al. (2009). Their longest period is approximatively our shortest period (Table 2). The short period data ought to be only marginally sensitive to structures at depths more than 1200 km which may explain our agreement in areas with many high quality observatories.

Lateral variation of seismic velocity and electrical conductivity result from temperature and compositional changes in the mantle in relation with global geodynamics. Kelbert et al. (2009) observe some degree of correlation between conductivity and seismic tomography models in the upper mantle transition zone. Good correlation or more precisely anti-correlation is expected when temperature variations are the leading process in a dry mantle (Shankland et al., 1993; Utada et al., 2009; Verhoeven et al., 2008). When temperature increases, the velocity decreases while the conductivity increases.

Several tomography models of the mid-mantle are available (e.g. Becker and Boschi, 2002; Romanowicz, 2003). Becker and Boschi (2002) have synthetized the common large scale features observed in P-wave and S-wave models into mean models reproduced in Figure 13 at 1220 km depth. Here we only show the longest wavelengths in the models ($l = 1-9$) for comparison with the conductivity model. For this comparison, we selected the model with the SH expansion form $l = 1-7$ (Figure 12) because the most abrupt conductivity constrasts are filtered out. Qualitatively, our mid-mantle conductivity model (Figure 13) shows some large scale common low conductivity-high velocity features with the tomography models, particularly beneath North and Central America, partly beneath South Astralia and to a less extent in South Africa, Japan, India and the Eastern part of Europe and North Africa. Common high conductivity - low velocity regions are observed as well in East Africa, part of Asia and Pacific though the later region was poorly constraint by a few observatories. Among the regions wtih reverse trends (i.e. high conductivity - high velocity or vice versa), we note the Indonesian region, Central Australia as well as the Western part of Europe and North Africa. A word

of caution is necessary. For instance, the quasi orthogonal trend observed in the South Atlantic near Africa (NW-SE in the conductivity model and NE-SW in the tomography models) may be the simple result of no magnetic observatory in the South Atlantic. In contrast, the trends observed in areas with observatories are probably robust. Hence, no correlation could be an indication of processes that act differently on conductivity and seismic velocity. A weak correlation between high conductivity and seismic velocity may be attributed for instance to water effect (Koyama et al., 2006).

We are getting close to obtain conductivity models that could be quantitatively compared to seismic data as well as geodynamic models. Some more work is still necessary to ascertain the full robustness of the features observed in Figures 12-13. There is also the need to estimate as precisely as possible the uncertainty in the conductivity parameters. Last but not least, we should be able to provide some description of the conductivity variation with depth if the data allowed it. The obvious step forward to address these questions is to update our database with observatory data from 1991-present.

6. Conclusion

We analyzed 32 years of magnetic monthly mean values from a worldwide set of geomagnetic observatory to infer the lower mantle electrical conductivity. Data were processed and inverted in the time and space domain and a vertically averaged laterally heterogeneous conductivity model in the depth range 900-1400 km was obtained. Large scale structures were revealed. Conductivity values vary by more than one order of magnitude between resistive regions and conductive domains. Several inversions were run on synthetic

and real data to explore the stability of the inversion and to obtain clues about model resolution. The conductivity changes in the lower mantle may be partly due to temperature and iron content changes when correlated to tomography models. Otherwise, other processes should be involved. The interpretation is limited by the lack of mineral physics studies of conductivity enhancement of lower mantle minerals by minor phases such as water or carbonates. Eventually, the robustness of our findings should be tested further with long data time series including the magnetic monthly mean values from 1991-present. However, while the most recent data are of improved quality in terms of measurement precision and baseline reliability, there are fewer observatories than before and major threats exist to close some of them. Finally, many more years of satellite data are necessary to obtain geomagnetic fields at periods long enough to probe the deep mantle.

References

Banks, R., 1969. Geomagnetic variations and the electrical conductivity of the upper mantle. Geophys. J. R. Soc., 17, 457-487.

Becker, T.W., Boschi, L., 2002. A comparison of tomographic and geodynamic mantle models. Geochem. Geophys. Geosyst., 3, 10.129/2001GC000168.

Beiner, J. ,1973. Analysis in phases of diffusion PI- C-12 beneath 300 MEV. Nuclear Physics, B53, 349-365.

Chave, A.D., Thompson, D.J., 1989. Some comments on magnetotelluric response function estimation. J. Geophys. Res., 94, 14215-14226.

Constable, S. Constable, C., 2004. Observing geomagnetic induction in magnetic satellite measurements and associated implications for mantle conductivity. Geochemistry, Geophysics, Geosystems, 5, doi:10.1029/2003GC000.634.

Courtillot, V., Le Mouel, J.L., 1988. Time variations of the earth's magnetic field: from daily to secular. Ann. Rev. Earth Planet. Sci., 16, 389-476.

Egbert,G.D., Booker,J.R., 1992. Very long period magnetotellurics at Tucson observatory: implications for mantle conductivity. J. Geophys. Res., 97, 15099-15112.

Fujii, I., Schultz, A., 2002. The 3D electromagnetic response of the earth to ring current and auroral oval excitation. Geophys. J. Int., 151, 689-709.

Grammatika, N., Tarits, P., 2002. Contribution at satellite altitude of electromagnetically induced anomalies arising from a three-dimensional heterogeneously conducting earth, using Sq as an inducing source field. Geophys. J. Int., 151, 913-923.

Hautot, S., Tarits, P., Whaler, K.A., Le Gall, B., Tiercelin, J.J, Le Turdu, C., 2000. The deep structure of the Baringo Rift basin (central Kenya) from 3-D magneto-telluric imaging: Implications for rift evolution, J. Geophys. Res., 105, 23493-23518.

Jackson, A., Jonkers, A.R.T, Walker, M.R.,2000. Four centuries of geomagnetic secular variation from historical records. Phil. Trans. London, A, 358(1768), 957-990.

Katsura, T., Sato K., Ito, E., 1998. Electrical conductivity of perovskite at lower-mantle conditions. Nature, 395, 493-495.

Kelbert, A., Egbert, G., Schultz, A., 2008. Non-linear conjugate gradient inversion for global EM induction: resolution studies. Geophys. J. Int., 173, 365-381.

Kelbert, A., Schultz, A., Egbert, G., 2009. Global electromagnetic induction constraints on transition-zone water content variations. Nature, 460, 1003-1006.

Koyama, T., Shimizu, H., Utada, H., Ichiki, M., Ohtani, E., Hae, R., 2006. Water content in the mantle transition zone beneath the North Pacific derived from thej electrical conductivity anomaly, AGU Geophys. Monogr. Ser., 168,171-179.

Kuvshinov, A., 2008. 3-D Global Induction in the Oceans and Solid Earth: Recent Progress in Modeling Magnetic and Electric Fields from Sources of Magnetospheric, Ionospheric and Oceanic Origin. Surveys Geophysics, 29 (2), 139-186.

Kuvshinov, A., Olsen, N., 2006. A global model of mantle conductivity derived from 5 years of CHAMP, Oersted, and SAC-C magnetic data. Geophys. Res. Lett, 31,DI 10.1029/2006GL027083.

Mandea Alexandrescu, M., Gibert, D., Le Mouel, J.L., Hulot, G., Saracco, G., 1999. An estimate of average lower mantle conductivity by wavelet analysis of geomagnetic jerk. J. Geophys. Res., 104, 17735-17745.

Mochizuki, E., Yokoyama,Y., Shmimizu, I., Hamano, Y., 1997. Spherical harmonic analysis in terms of unevenly distributed observation points and its applications to geomagnetic data. J. Geomag. Geoelecr., 49, 1013-1033.

Olsen, N., 1999. Induction studies with satellite data. Surv. Geophys., 20(34), 309-340.

Ohta, K., Onoda, S., Hirose, K., Sinmyo, R., Shimizu, K., Sata, N., Ohishi, Y., Yasuhara, A., 2008. The electrical conductivity of post-perovskite in earth's D" layer. Science, 320, 89-91.

Parker, R.L., 1980. The inverse problem of electromagnetic induction: Existence and construction of solutions based on incomplete data. J. Geophys. Res. 85, 44214428.

Romanowicz, B., 2003. Global mantle tomography: progress status in the past 10 years. Ann. Rev. Earth Planet., 31, 303-328.

Schultz, A., Larsen, J.C., 1990. On the electrical conductivity of the mid-mantle: II. Delineation of heterogeneity by application of extremal inverse solutions, Geophys. J. Int., 101, 565580

Schultz,A., Kurtz, R.D., Chave, A.D., Jones, A.G., 1993. Conductivity discontinuities in the upper mantle beneath a stable craton. Geophys. Res. Lett., 20, 2941-2944.

Semenov, V.Y., Jozwiak,W., 1999, Model of the geoelectrical structure of the mid- and lower mantle in the Europe-Asia region. Geophys. J. Int., 138, 549-552.

Semenov, V.Y., Jozwiak, W., 2006. Lateral variations of the mid-mantle conductance beneath Europe. Tectonophysics, 416, 279-288.

Shankland,T.J., Peyronneau, J., Poirier J.-P., 1993. Electrical conductivity of the Earth's lower mantle. Nature, 366, 453-455.

Tarits, P., Wahr, J., Lognonné P., 1992. Electrical conductivity heterogeneities in the Mantle: correlation with mantle velocity structure. AGU, San Francisco, abstract.

Tarits,P., 1994. Electromagnetic studies of global geodynamic processes. Surv. Geophys., 15(9), 209-238.

Utada,H.,Koyama,T, Shimizu, H., Chave,A.D., 2003. A semi global reference model for electrical conductivity in the mid-mantle beneath the north Pacific region, Geophys. Res. Lett., 30, 1194, doi:10.1029/2002GL016092.

Utada, H., Koyama, T., Obayashi, M., Fukao, Y., 2009. A joint interpretation of electromagnetic and seismic tomography models suggests the mantle transition zone below Europe is dry. Earth Planet. Sci. Lett., 281, 249-257.

Uyeshima, M., Schultz, A., 2000. Geoelelectromagnetic induction in a heterogeneous sphere: a new 3D forward solver using a staggered-grid integral formulation. Geophys. J. Int., 140, 636-650.

Verhoeven, O., Vacher, P., Mocquet, A., Rivoldini, A.,Menvielle, M., Arrial, P.A., Choblet, G., Tarits, P., Dehant, V., Van Hoolst, T., 2009. Constraints on thermal state and composition of the Earth's lower mantle

588 from electromagnetic impedances and seismic data. J. Geophys. Res., 114,
589 DOI10.1029/2008JB005678

590 Weidelt, P., 1972. The inverse problem of geomagnetic induction. Zeitschrift
591 fur Geophysik, 38, 257-289.

592 Xu,Y., Shankland, T.J., Poe,B.T., 2000. Laboratory-based electrical conduc-
593 tivity in the Earth's mantle. J. Geophys. Res., 105, 27865-27875.

Table 1: List of geomagnetic observatory: IAGA code and geographical location.

Obs.	Lat	Long	Obs.	Lat	Long	Obs.	Lat	Long
aaa	43.15	76.55	aae	9.03	38.76	abg	18.64	72.87
agn	43.74	280.73	aia	-65.25	295.74	ale	82.50	297.65
aml	-43.15	172.72	ams	-37.83	77.57	ann	11.37	79.68
api	-13.81	188.23	aql	42.38	13.32	ars	56.43	58.43
bdv	49.08	14.02	bel	51.84	20.79	bfe	55.63	11.67
bji	40.04	116.18	blc	64.33	263.97	bng	4.44	18.57
bou	40.14	254.76	brw	71.32	203.38	bsl	40.50	339.26
cbb	69.20	255.00	clf	48.02	2.27	cmo	64.86	212.16
cnb	-35.31	149.36	cnh	44.05	125.21	coi	40.22	351.58
crp	10.44	275.09	czt	-46.43	51.87	dlr	29.49	259.08
dob	62.07	9.12	dou	50.10	4.59	drv	-66.67	140.01
ebr	40.82	0.49	esk	55.32	356.80	eyr	-43.42	172.35
fcc	58.67	265.91	frd	38.21	282.63	frn	37.10	240.30
fuq	5.47	286.26	fur	48.17	11.28	gdh	69.25	306.47
gln	49.63	262.90	gna	-31.78	115.95	gua	13.58	144.87
gzh	23.09	113.34	had	50.99	355.52	hbk	-25.88	27.71
her	-34.42	19.23	hlp	54.61	18.82	hon	21.32	202.00
hrb	47.87	18.19	hua	-12.05	284.67	hyd	17.41	78.56
irt	52.17	104.45	isk	29.07	38.32	kak	36.23	140.19
kiv	50.72	30.30	kny	31.42	130.88	kod	10.23	77.46
krc	24.95	67.14	las	-35.01	302.31	ler	60.13	358.82
lnn	59.95	30.70	lov	59.35	17.83	lrv	64.18	338.30
lvv	49.90	23.75	lzh	36.09	103.85	mab	50.30	5.68
maw	-67.61	62.88	mbc	76.20	240.60	mbo	14.39	343.04
mcq	-54.50	158.95	mea	54.62	246.67	miz	39.01	141.08
mmb	43.91	144.19	mmk	68.25	33.08	mnk	54.50	27.88
mos	55.47	37.31	naq	61.10	314.80	nck	47.63	16.72
new	48.26	242.88	ngk	52.07	12.68	nur	60.51	24.66
nvs	55.03	82.90	ode	46.78	30.88	ott	45.40	284.45
paf	-49.35	70.26	pag	42.22	24.18	pbq	55.28	282.26
pmg	-9.41	147.15	pod	61.60	90.00	ppt	-17.57	210.43
res	74.70	265.10	sab	30.36	77.80	sba	-77.85	166.78
sit	57.06	224.68	sjg	18.11	293.85	sod	67.37	26.63
spt	39.55	4.35	ssh	31.10	121.19	stj	47.60	307.32
sua	44.68	26.25	tfs	42.09	44.71	thl	77.48	290.83
thy	46.90	17.89	too	-37.53	145.47	trd	8.48	76.95
trw	-43.25	294.68	tsu	-19.22	17.70	tuc	32.25	247.17
val	51.93	349.75	vic	48.52	236.58	vss	-22.40	316.35
whn	30.53	114.56	wik	48.26	16.32	wit	52.81	6.67
wng	53.74	9.07	yak	62.02	129.72	ykc	62.48	245.52

Table 2: One-dimensional C-response for the P_0^1 geometry (geomagnetic dipole). Period (T) is in months.

T (mo.)	Re(C) km	Im(C) km	Σ km
21.3	1926.8	-632.3	119.0
16.0	1713.5	-580.7	238.5
10.7	1693.2	-1124.6	446.6
8.0	1523.2	-400.3	111.0
5.3	1469.4	-370.8	73.5
4.0	1164.7	-408.2	52.3
2.7	1112.9	-210.3	58.9

Table 3: Conductivity model used to synthesize the synthetic data. Layer 3 is heterogeneous (het.) .

Layer	Conductivity (S/m)	Depth range (km)
1	0.01	0-660
2	0.1	660-900
3	het.	900-1400
4	3.3	1400-2400
Core	25	-

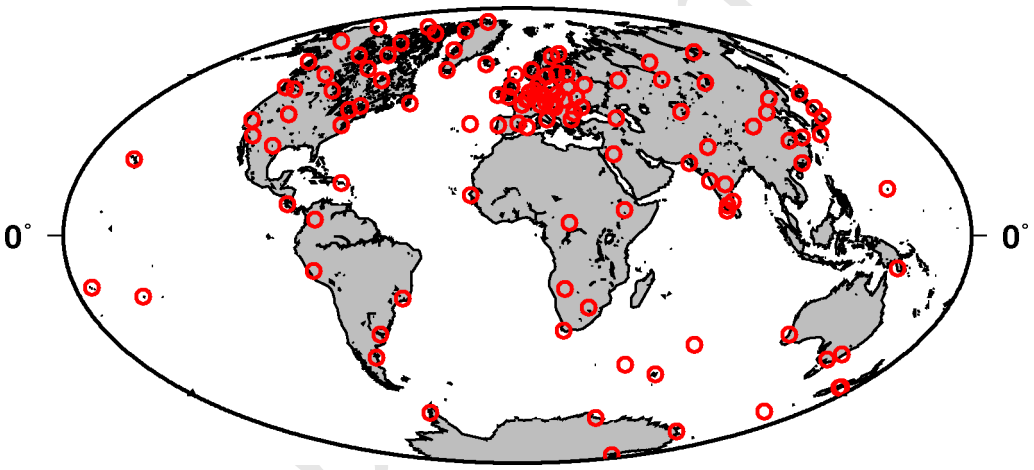

Figure 1: Worldwide distribution of geomagnetic observatories used in this study.

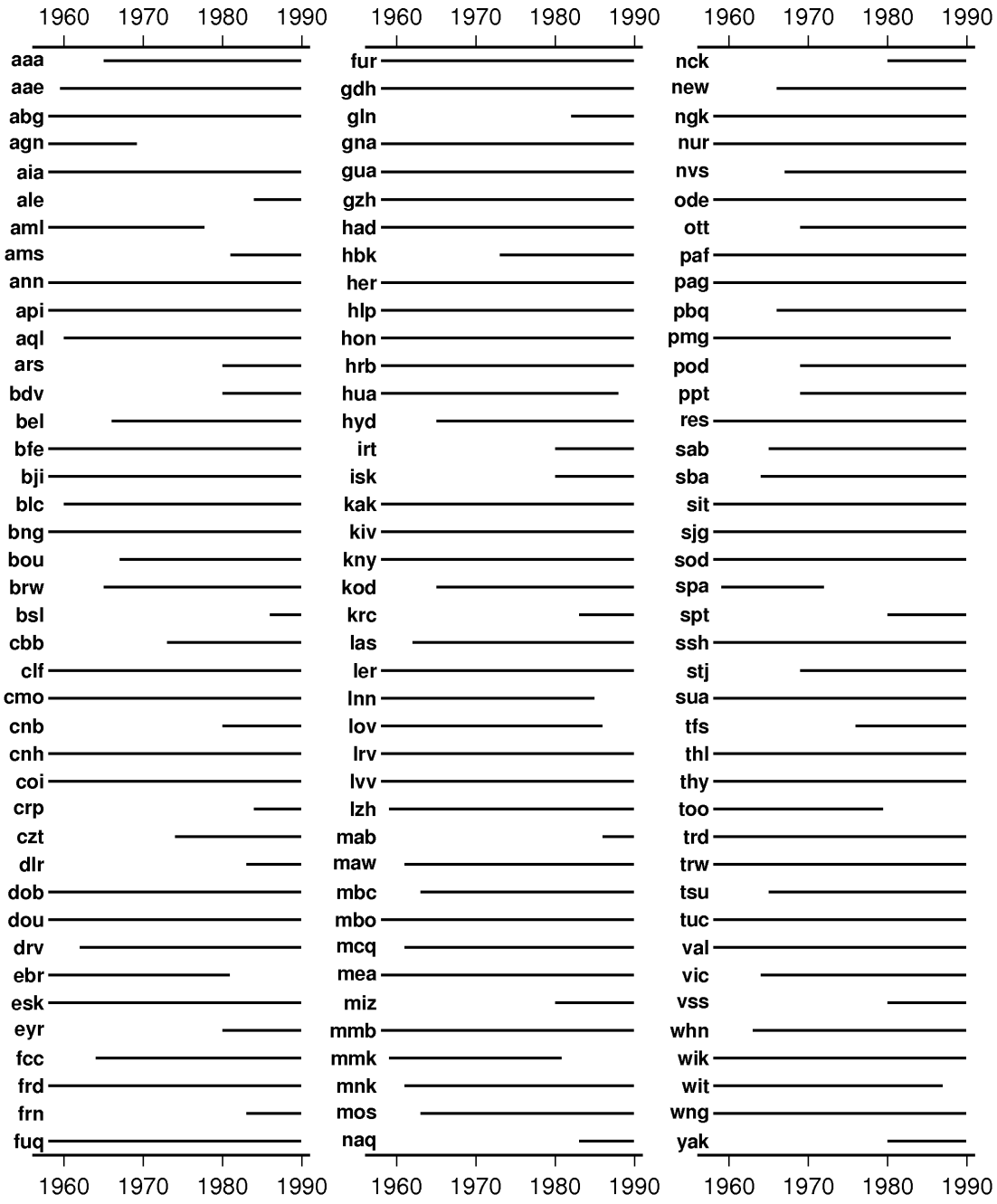

Figure 2: Data duration for each observatory (horizontal black line).

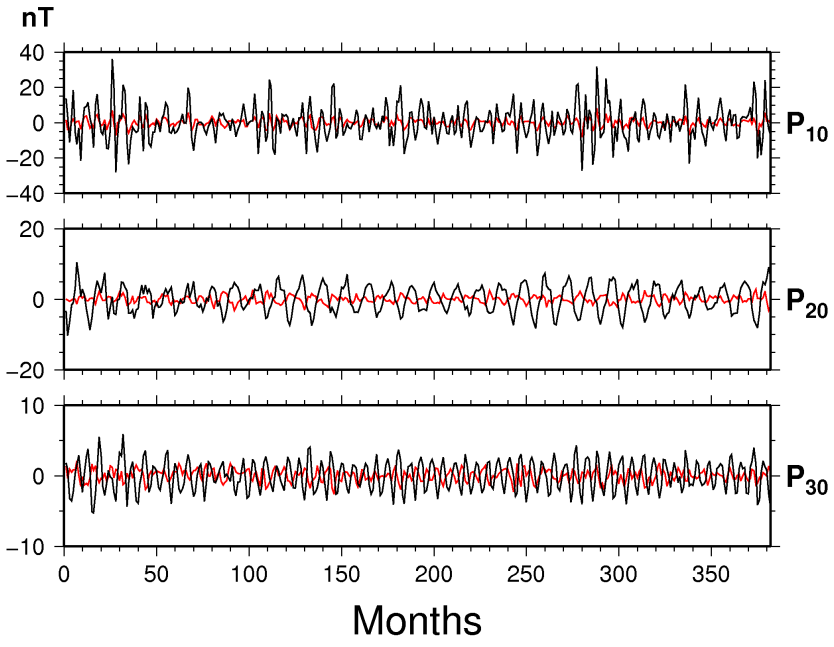

Figure 3: Time series of the zonal ($l = 1-3$) spherical harmonic coefficients of the external (black) and internal (red) magnetic potentials obtained from the global SH analysis of the monthly mean data.

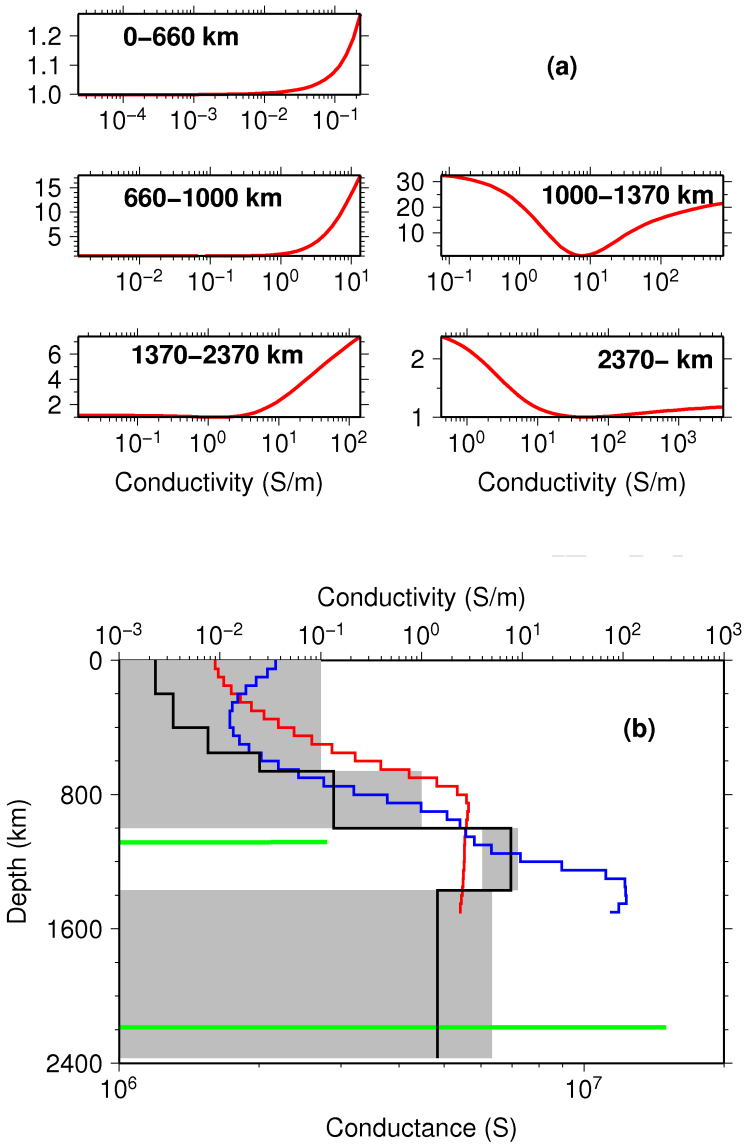

Figure 4: (a) Conductivity profile and depth resolution for the data set in Table 2. For each layer, the graph shows the χ^2 misfit against the conductivity values in this layer. The ordinate axis is χ^2 divided by its minimum value. (b) Conductivity profiles versus depth. The shaded area corresponds to the values in (a). In black a 1-D profile obtained for a 7 layers model. The Dirac conductances are shown in green, the model by Kuvshinov and Olsen (2006) in red and by Constable and Constable (2004) in blue.

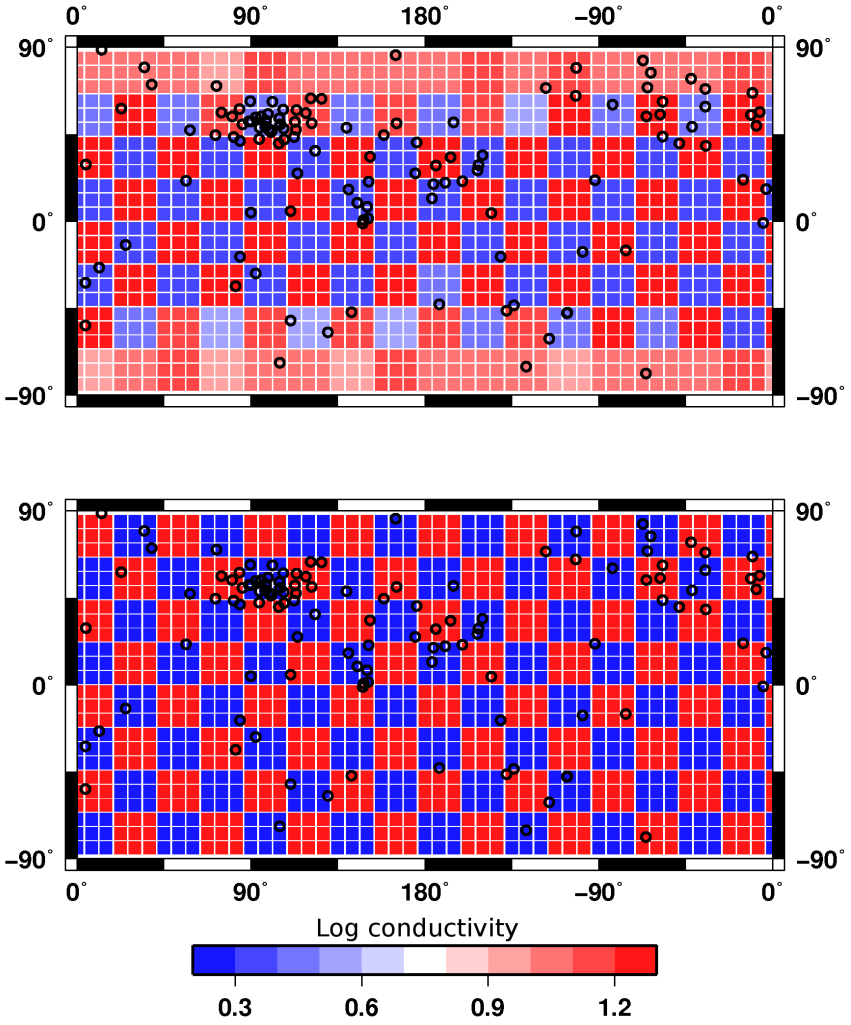

Figure 5: Checkboard model. Bottom: original conductivity structure; Top: inverse solution. The open circles are the position of the sites where the synthetic data were synthesized. See text for details.

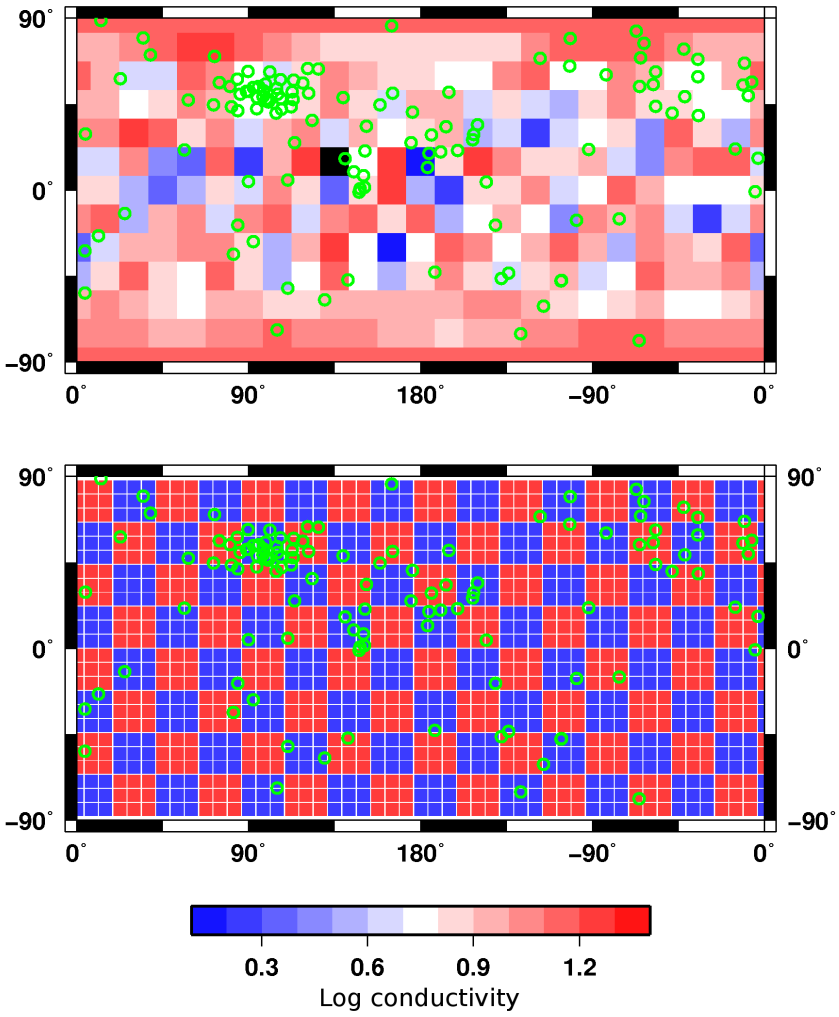

Figure 6: Checkboard model. Bottom: original conductivity structure; Top: inverse solution. The open circles are the position of the sites where the synthetic data were synthesized. See text for details.

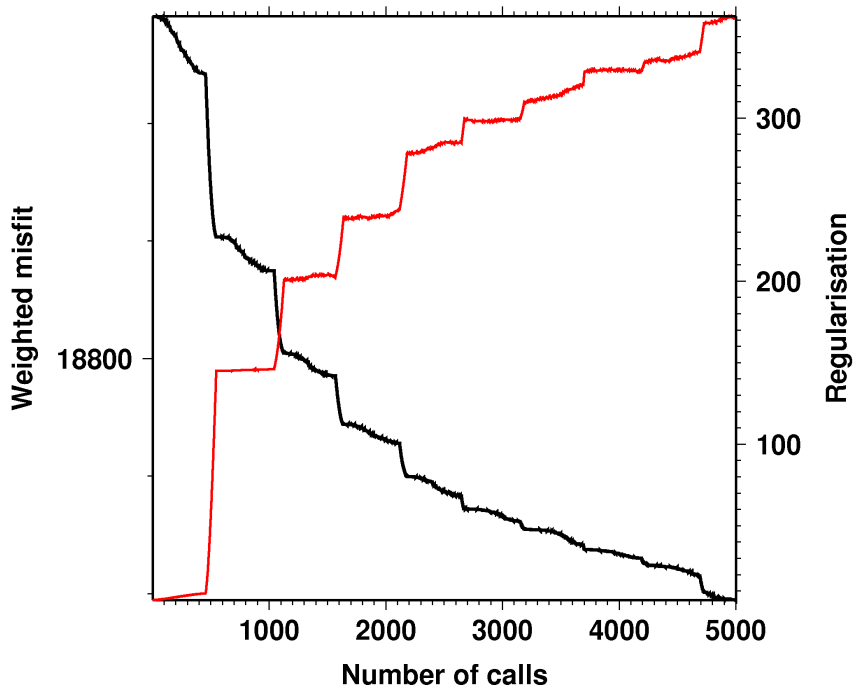

Figure 7: Evolution of the misfit function with respect to the number of calls to the forward solver. The weighted misfit is in black and the regularisation term in red. The units are arbitrary.

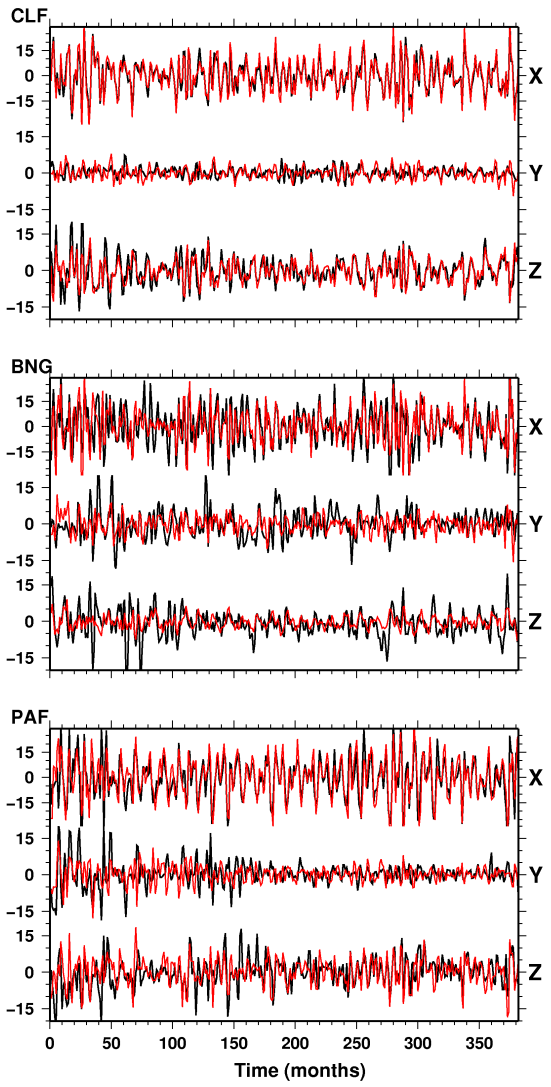

Figure 8: Example of fit for three observatories. For each observatory, X is the north magnetic component, Y the east magnetic and Z the vertical component positive downward. The horizontal field is in the geomagnetic reference frame. The data are in black and the model in red.

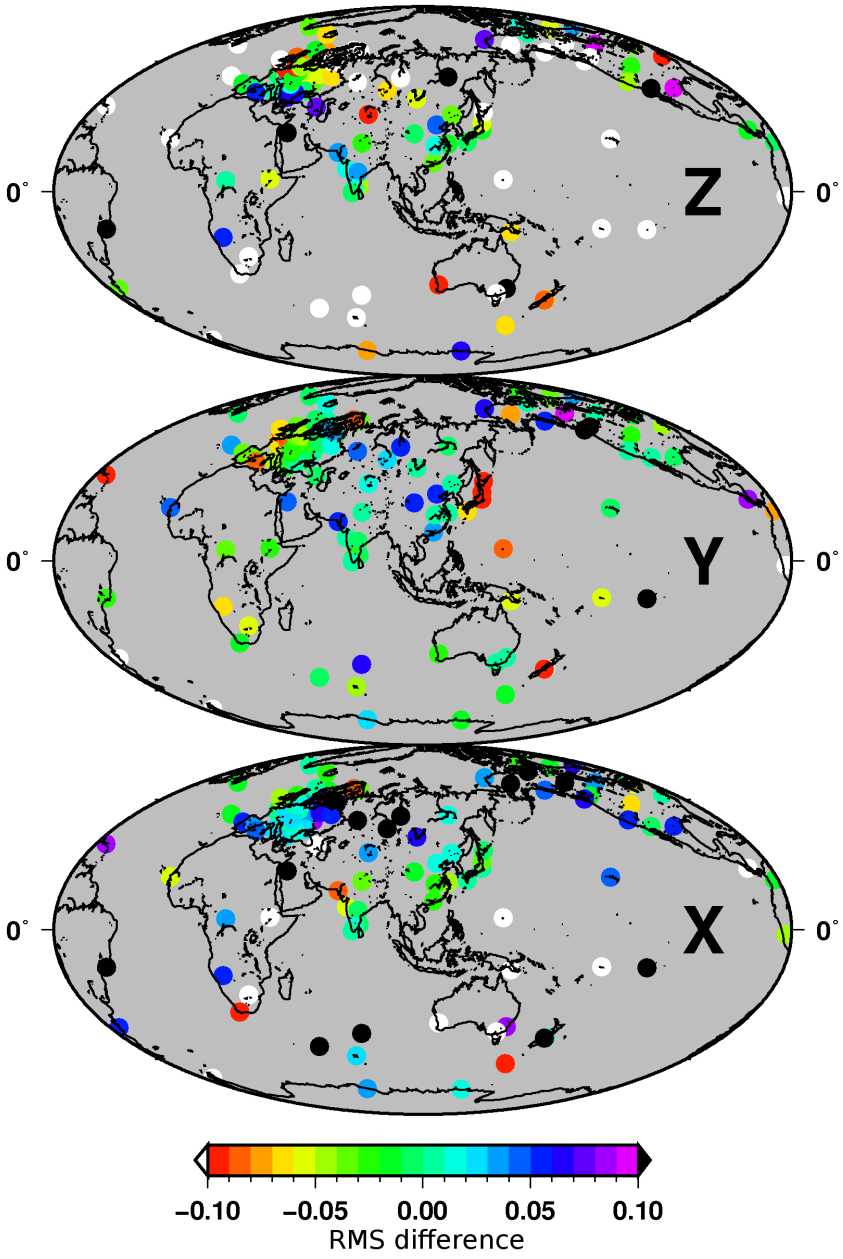

Figure 9: Global distribution of *rms* differences at all observatories and each component between the final inverse solution and the 1-D solution. See text for the definition of *rms*.

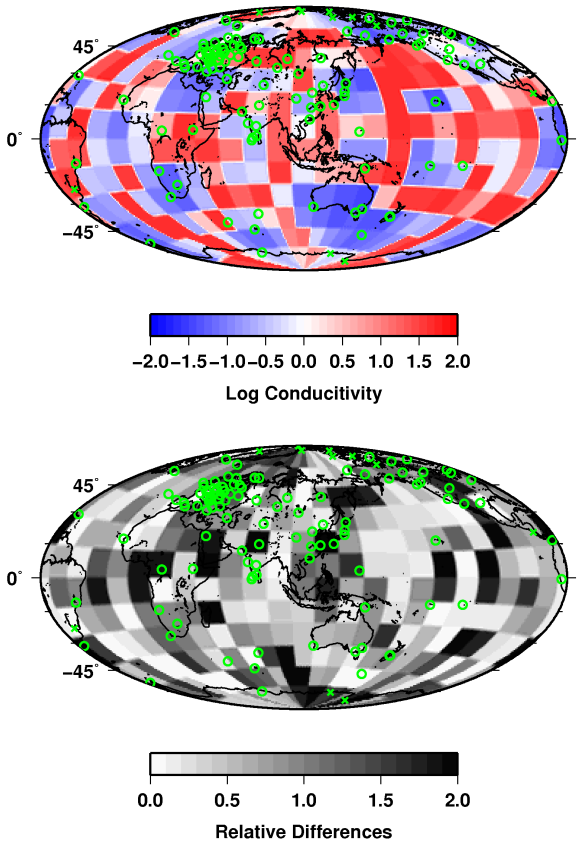

Figure 10: Top: Conductivity map for layer 3. This model is the average of two models obtained separately with two different 1-D starting values; Bottom: map of the relative conductivity difference (Δ) between the two models. The Δ value is the absolute value of the difference between two conductivities in one mesh divided by the mean value in that mesh. The open circles are the observatories used in the inversion and the crosses the observatories discarded (see text). The maps are in the geomagnetic reference frame.

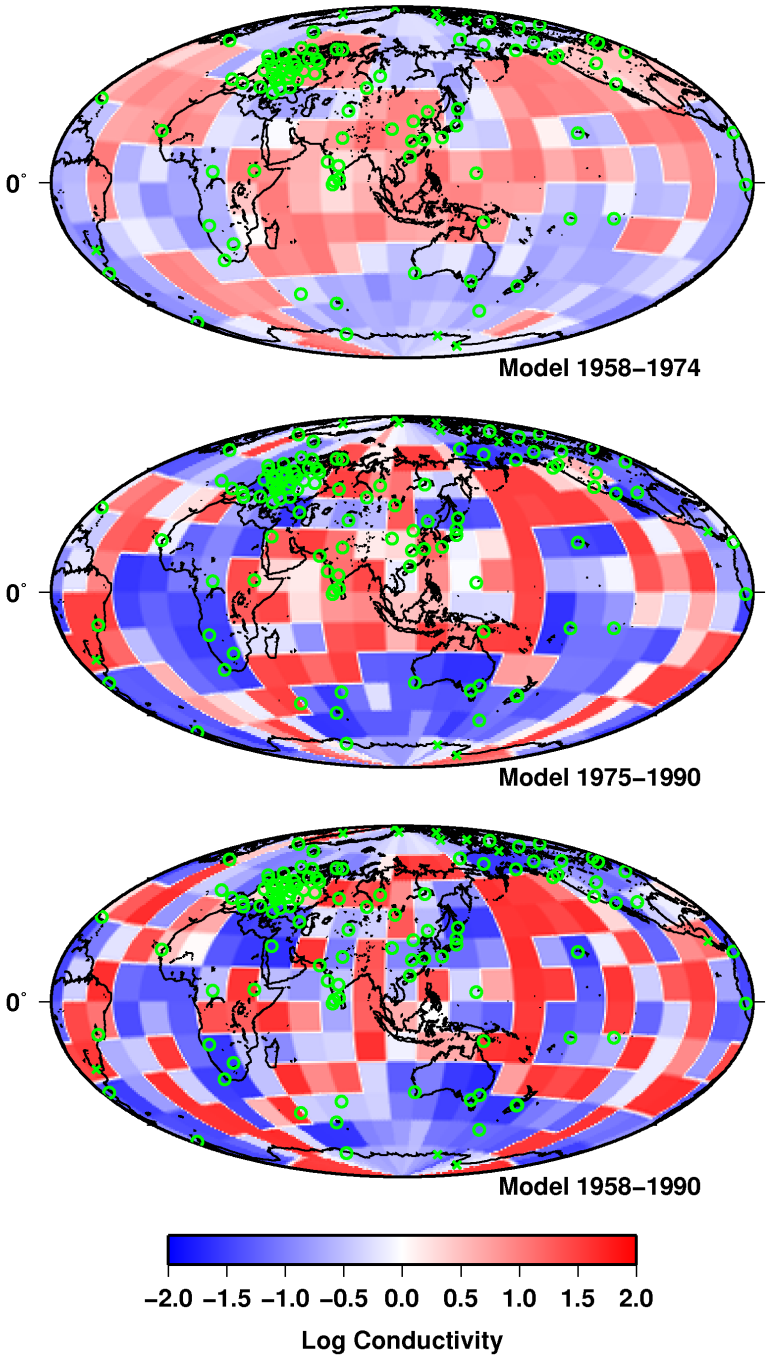

Figure 11: Maps of conductivity models obtained with data from 1958-1974 with 97 observatories (top), from 1975-1990 (middle) with 119 observatories and for the whole time series (1958-1990). For all 3 models, the 1-D initial conductivity value was 1.8 S/m. The maps are in the geomagnetic reference frame.

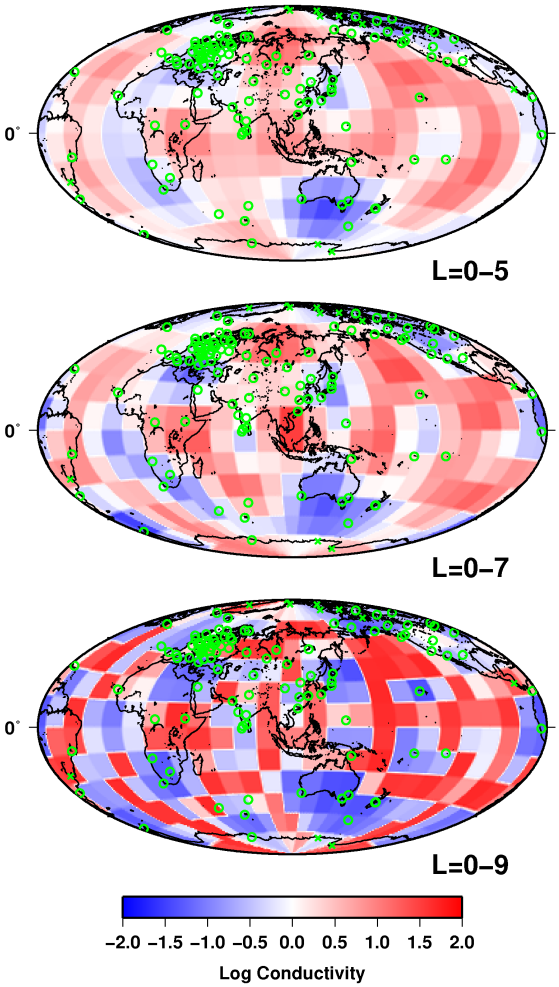

Figure 12: Conductivity maps at different wavelength. The wave length decreases from top to bottom with a maximum SH degree of $l = 5$ (top), $l = 7$ (middle),$l = 9$ (bottom). The maps are in the geomagnetic reference frame.

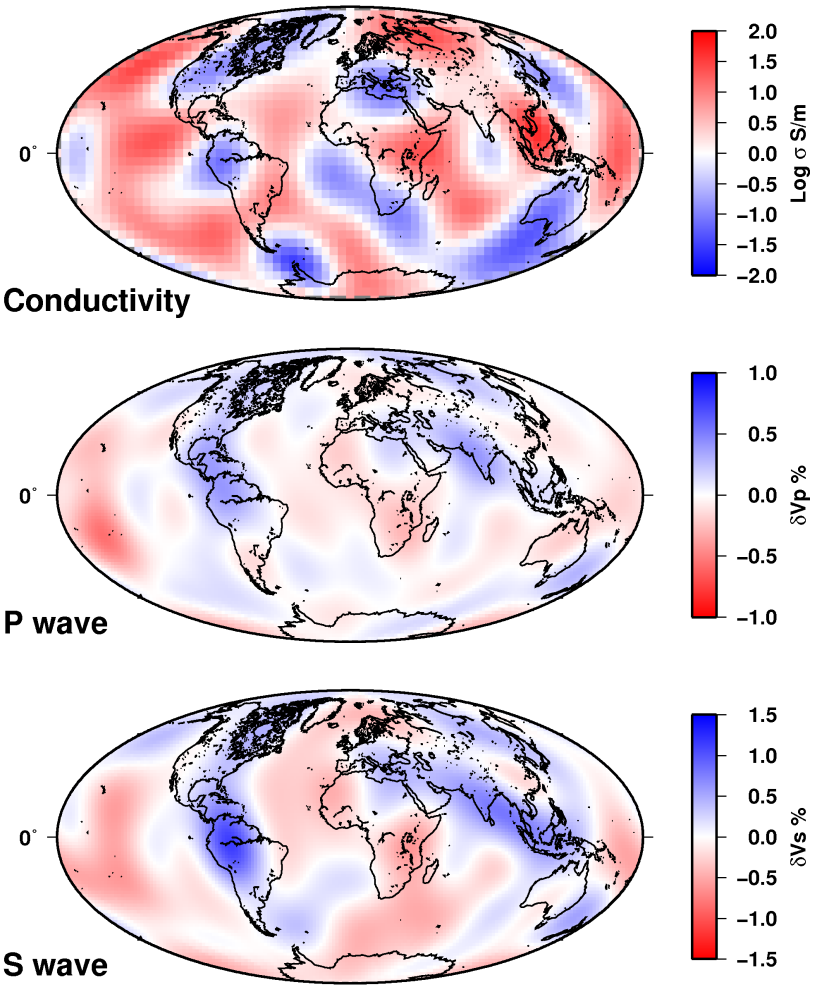

Figure 13: The upper map is the conductivity model from l=0-7 from Figure 12. The model was rotated into geographical coordinates and resampled for plotting. The two bottom maps are the tomography models for P wave and S-wave from (Becker and Boschi, 2002) at depth 1220 km recalculated at $l = 1 - 9$.